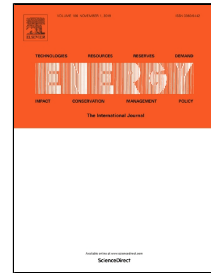


# Journal Pre-proof

Modeling of heat transfer for energy efficiency prediction of solar receivers

J. Zhu, K. Wang, Z. Jiang, B. Zhua, H. Wu



PII: S0360-5442(19)32067-5  
DOI: <https://doi.org/10.1016/j.energy.2019.116372>  
Reference: EGY 116372

To appear in: *Energy*

Received Date: 25 October 2018  
Accepted Date: 15 October 2019

Please cite this article as: J. Zhu, K. Wang, Z. Jiang, B. Zhua, H. Wu, Modeling of heat transfer for energy efficiency prediction of solar receivers, *Energy* (2019), <https://doi.org/10.1016/j.energy.2019.116372>

This is a PDF file of an article that has undergone enhancements after acceptance, such as the addition of a cover page and metadata, and formatting for readability, but it is not yet the definitive version of record. This version will undergo additional copyediting, typesetting and review before it is published in its final form, but we are providing this version to give early visibility of the article. Please note that, during the production process, errors may be discovered which could affect the content, and all legal disclaimers that apply to the journal pertain.

© 2019 Published by Elsevier.

# Modeling of heat transfer for energy efficiency prediction of solar receivers

J. Zhu<sup>a</sup>, K. Wang<sup>b</sup>, Z. Jiang<sup>b</sup>, B. Zhu<sup>a</sup>, H. Wu<sup>c,\*</sup>

<sup>a</sup>National Key Laboratory of Science and Technology on Aero-Engine Aero-thermodynamics, Collaborative Innovation Center of Advanced Aero-Engine, School of Energy and Power Engineering, Beihang University, Beijing, 100191, China

<sup>b</sup>Institute of Engineering Thermophysics, Chinese Academy of Sciences, Beijing, 100190, China

<sup>c</sup>School of Engineering and Technology, University of Hertfordshire, Hatfield, AL10 9AB, United Kingdom

\*Corresponding author. Email: h.wu6@herts.ac.uk Tel. +44(0)1707 284265; Fax. +44(0)1707 285086

## Abstract

In this article, a new heat transfer model for solar receivers with metal foam is developed for design optimization. The proposed model facilitates analysis of heat transfer processes in terms of forced convection, natural convection, heat conduction and radiation, accurately predicting the energy efficiency and percentage contribution of each form of heat loss. The results show good agreement between the predicted results and the experimental data. Specifically, sensitivity analysis is performed to predict the energy efficiency of solar receivers under different operating conditions. To explore the influence of inlet temperature, a series of simulations under high inlet temperature are carried out, resulting in poorer energy performance and heavier radiant heat loss. Non-radiant heat loss, however, accounts for less than 1.1% of the total energy loss in all cases. The results reveal that reduction of radiant loss is conducive to energy efficiency improvement.

**Key Words:** Solar receiver, modeling, energy efficiency, metal foam, radiation

## Nomenclature

|                   |   |                   |   |
|-------------------|---|-------------------|---|
| $A_1$             | surface area of phase 1 (m <sup>2</sup> )   | $A_f$             | area of the Ni-foam (m <sup>2</sup> )   |
| $A_g$             | area of quartz glass at the wavelength of visible light (m <sup>2</sup> )                             | $A_{sf}$          | surface area heat transfer coefficient of the Ni-foam (m <sup>2</sup> )                               |
| $A_w$             | area of the inner cylinder wall of the front part of the Ni-foam (m <sup>2</sup> )                    | $A_c$             | shadow area of the concentrator(m <sup>2</sup> )  |
| $C_{av}$          | average heat capacity of air inlet and outlet (J·kg <sup>-1</sup> K <sup>-1</sup> )                   | $C_{p,c,1}$       | average specific heat capacity of the air in cold end in phase 1(J·kg <sup>-1</sup> K <sup>-1</sup> ) |
| $C_{p,h,1}$       | average specific heat capacity of the air in hot end in phase 1(J·kg <sup>-1</sup> K <sup>-1</sup> )  | $C_{p,2}$         | average specific heat capacity of the air in phase 2(J·kg <sup>-1</sup> K <sup>-1</sup> )             |
| $C_{p,3}$         | average specific heat capacity of the air in phase 3(J·kg <sup>-1</sup> K <sup>-1</sup> )             | $C_{p,4}$         | average specific heat capacity of the air in phase 4 (J·kg <sup>-1</sup> K <sup>-1</sup> )            |
| $F_{fg}$          | radiation shape factor between foam and glass   | $F_{fw}$          | radiation shape factor between foam and the wall of the inner cylinder                                |
| $F_{wg}$          | radiation shape factor between surface of inner cylinder and glass                                    | $G$               | instantaneous solar radiation density (W/m <sup>2</sup> )   |
| $h_{gi}$          | convective heat transfer coefficients of the inner surface of the quartz glass (W/(m <sup>2</sup> K)) | $h_{go}$          | convective heat transfer coefficients of the outer surface of the quartz glass (W/(m <sup>2</sup> K)) |
| $h_{sf}$          | convective heat transfer coefficient of the Ni-foam (W/(m <sup>2</sup> K))                            | $I_b$             | energy entering the solar receiver (J)  |
| $k_1$             | heat transfer coefficient for phase 1 (W/(m <sup>2</sup> K))  | $\dot{m}$         | mass flow rate (kg/s)   |
| $Q_r$             | energy absorbed by the receiver (J)   | $T_{34}$          | average of temperature $T_3$ and $T_4$ (°C)   |
| $T_a$             | ambient temperature(°C)   | $T_f$             | temperature of the Ni-foam (°C)   |
| $T_g$             | temperature at the wavelength of visible light (°C)   | $T_i$             | temperature of inlet (°C)   |
| $T_o$             | temperature of outlet (°C)  | $\Delta T_{\max}$ | maximum between $(T_o - T_i)$ and $(T_4 - T_1)$ (°C)  |
| $\Delta T_{\min}$ | minimum between $(T_o - T_i)$ and $(T_4 - T_1)$ (°C)  | $T_w$             | temperature of the inner cylinder wall of the front part of the Ni-foam (°C)                          |
| $\alpha_g$        | absorbance at the wavelength of visible light   | $\alpha'_g$       | absorbance of quartz glass under long wave  |

|                 |  |                  |  |
|-----------------|--|------------------|--|
| $\varepsilon_f$ | emissivity of the Ni-foam  | $\varepsilon_g'$ | emissivity of quartz glass under long wave   |
| $\varepsilon_w$ | emissivity of the inner cylinder wall of the front part of the Ni-foam | $\eta_c$         | specular reflection efficiency of the concentrator                                       |
| $\rho_f$        | reflectivity of the Ni-foam  | $\sigma$         | blackbody radiation intensity( $5.67 \times 10^{-8}$ W/(m <sup>2</sup> K <sup>4</sup> )) |
| $\tau_g$        | transmittivity at the wavelength of visible light                      | $\Phi_1$         | specific heat absorbed by the air in phase 1 (W)   |

## 1. Introduction

Fossil fuel scarcity and the ever-worsening global warming nurture research and development of the renewable energy, among which solar energy is commonly recognized as one of the most promising candidates [1]. As one of the massive utilizing directions, the Concentrated Solar Power (CSP) system transfers solar energy into thermal energy, and finally into mechanical power (integration of the CSP system and Brayton micro-turbines is one example [2, 3]). Solar receiver, one of the key components in CSP, works as a special energy exchanger to convert solar irradiation energy into thermal energy [4]. The thermal load of solar receivers could be significantly high, i.e. 1 MW is the central receiver system funded by the Ministry of Sciences and Technology of the People's Republic of China, set in Beijing in 2009 [5]. In the PEGASE (Production of Electricity by Gas Turbine and Solar Energy) project, the CNRS/PROMES laboratory developed a 4 MW pressurized air solar receiver based on compact heat exchanger technology [6]. ETH Zurich and Paul Scherrer Institute conducted a field test on a 42 meters long full-scale solar receiver prototype installed on a 9 m-aperture solar trough concentrator. The efficiency of the receiver ranged from 29% to 45% with solar power input of 280 kW [7-9]. The results indicate high correlation between solar receivers' energy efficiency & total pressure loss and the system's efficiency and cost [10-12]. The collected thermal energy was transferred to

other components in the system by circulating medium. To enhance heat transfer performance and reduce the dimension of the solar receiver, porous medium could be introduced as the collector medium. Metal foam is prevailing due to its high porosity (>95%), large specific surface area (>5000 m<sup>-1</sup>), high mechanical strength and low cost [13, 14]. The design optimization of the solar receiver is, however, still challenging due to the complexity of porous medium. Mendes et al. [15] proposed a simplified two-parameter model for effective thermal conductivity of open-cell porous foams. It was reported that the simplified model could predict the effective thermal conductivity of all the investigated structures in case of correct application of thermal conductivity ratio in each phase. By modeling differing virtual isotropic structures and performing 3-D direct numerical simulations, Kumar and Topin [16] generated a database of 2000 values about effective thermal conductivity. They studied the database to find the relationship between geometrical parameters and the effective thermal conductivity and built two models to predict the effective thermal conductivity, achieving excellent agreement between numerical and experimental data. The porous medium used in solar receivers has also been investigated. Buck et al. [17] conducted a performance test and retrofitted a receiver with new secondary concentrator. Several configurations of solar-hybrid gas turbine cycles in the low-medium power range were examined in terms of performance and cost. Albanakis et al. [18] tested different materials of porous medium and evaluated the receiver performance under varying operating conditions, demonstrating that Nickel foam bears better thermal property than the other foams. Michailidis et al. [19] employed the Ni-foam as porous medium in solar receivers and identified that the efficiency of the receiver depended on the geometrical parameters of the metal foam.

As experimental investigations cost high and last short, numerical simulation also plays an

important role in design and optimization phase. He et al. [20] established a coupled heat transfer model based on the Monte Carlo Ray Trace (MCRT) and Finite Volume Method (FVM) to predict the thermal behaviour in a parabolic trough solar receiver system. The average relative error was identified less than 2% by comparing the predicted outlet temperature with that of the experimental results. Wu et al. [21] presented a coupled heat transfer model to calculate the unsteady heat conduction of porous medium in solar receivers, which was proved as an efficient tool for receiver performance prediction. Chen et al. [22] examined the effect of various combinations of porosities and pore-sizes of porous medium on heat transfer performance. Hischier et al. [23] proposed a theoretical receiver model and conducted numerical calculation on a solar receiver used in a power generation system with combined Brayton-Rankine cycles [24]. Parametrical studies on temperature distribution and thermal efficiency have also been performed. The optimum predicted configuration was set and corresponding experimental investigations conducted [23]. After repeated design and test [25], a complete receiver with an output power of 35 kW was constructed and tested [26]. In addition, Lim et al. [27] designed a model for a tube-typed receiver by studying heat transfer characteristics and pressure drop characteristics based on discussion of the model and the optimum design. Weigal [28] also established a receiver model to analyze the measured efficiency value of solar receivers, which was lower than the designed one. Mortazavi [29] developed multi-scale modeling techniques to explore the thermal management efficiency of rechargeable batteries by employing paraffin composite structures.

It can be revealed from the above studies that modeling of heat transfer in solar receivers is important for development and optimization of the component as well as the energy system. To the best knowledge of the authors, few research has been reported to explore the heat transfer

process in solar receivers with porous medium taking forced convection, natural convection, heat conduction and radiation into account. Currently, a new heat transfer model for solar receivers with porous medium has been developed for design optimization, which has been validated by experimental data. Corresponding sensitivity analysis has also been carried out, providing reference for solar receiver design improvement. It is expected that the proposed model will be highly conducive to accurate prediction of the efficiency of heat exchanger under differing operating conditions.

## **2. Establishment of heat transfer analyzing model**

### *2.1. Configuration of solar receiver*

Fig. 1 presents a pressurized volumetric solar receiver in current CSP system, Fig. 1(a) a cross-sectional view of the receiver, and Fig. 1(b) a 3D view of the model. The advantage of the pressurized volumetric solar receiver lies in its high outlet air temperature and high thermal efficiency, although cooling of the light-incident glass and the flow balance in the heat absorbing core were two challenging problems in the process. The light-incident glass is made of quartz glass that can endure the maximum temperature of 1200 °C, yet when the concentrated solar directly focused on the glass, mechanical failure of cooling may occur. As a solution, the inlet air with relatively low temperature flowed through the glass as coolant, both extending the receiver's service life and reducing the probability of mechanical failure. Therefore, a large 50mm-diameter inlet tube was adopted, into which the pressurized air was injected and then separated into three 20mm-diameter branches. Welded on the back-side flange of the pressure cavity, the three smaller tubes were equally distributed in circumferential direction. Then, the air flowed through the gap between the internal and external cavities to the front region of the chamber and impinged onto the

quartz glass.

The main part of the receiver is 400 mm in diameter and 360 mm in height. The concentrated solar radiation (CSR) passed through the quartz glass and heated the absorbing core, which was made of Nickel foam that could endure the maximum temperature of 1453 °C. To increase the absorbing capacity, a 65mm-thick Nickel foam with the PPI (Pores per Inch) value of 75 and pore diameter of 0.34 mm was selected. Normally, smaller pore diameter entails larger heat transfer area and higher mean heat transfer coefficient. At last, to minimize heat loss, the receiver was surrounded by Aluminum silicate whose heat conductivity coefficient reached 0.06 W/(m·°C).



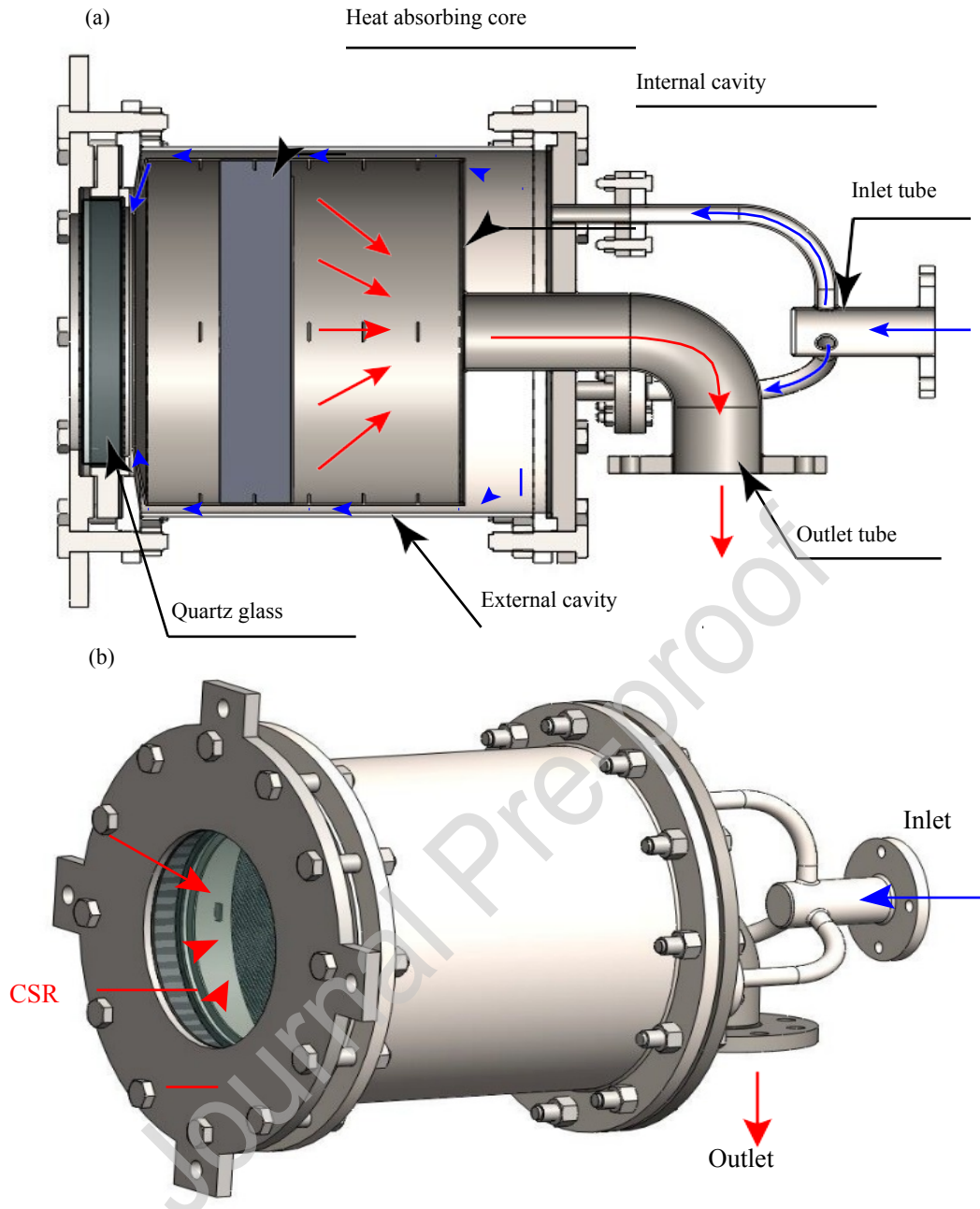


Figure 1 (a) Cross-section view of the receiver. (b) 3D view of the pressurized volumetric solar receiver.

## 2.2. Energy balance equation

A simplified model (Fig. 2) was established to calculate the steady-state heat transfer efficiency by analyzing heat loss. It is assumed that the solar radiation transmitted through the quartz glass window into the solar receiver's cavity is entirely irradiated on the surface of the metal foam, which is a uniform medium, and the air constitutes ideal gas. The heat transfer process is analyzed from the following five steps.

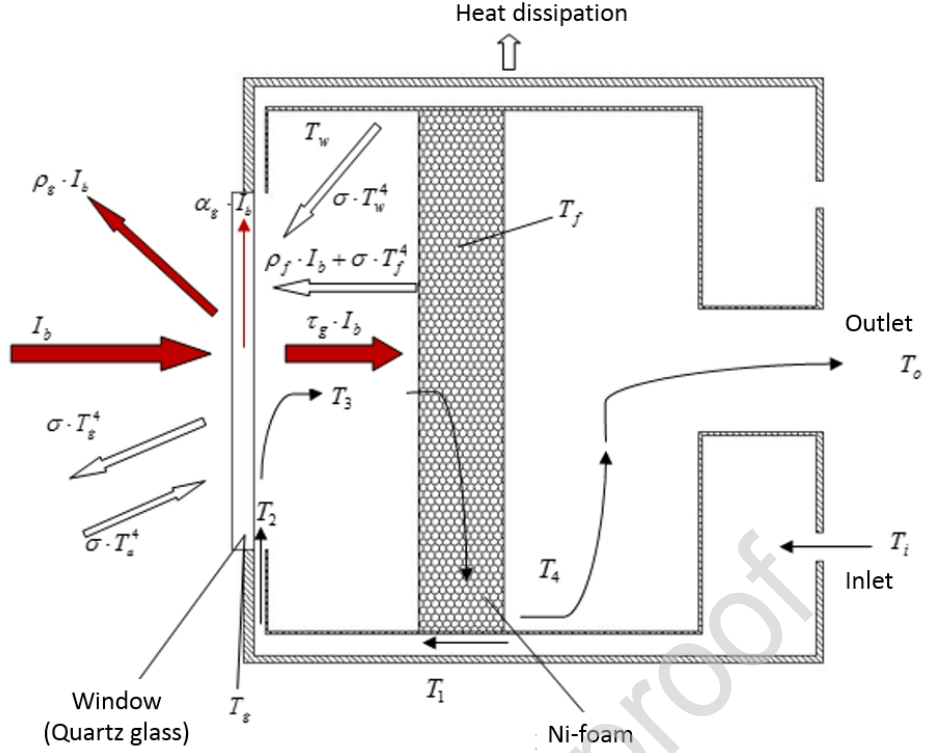


Figure 2 Simplified heat transfer model.

Initially, in the process of  $T_i \rightarrow T_1$ , the cooling air flows into the inlet and is heated by the foam through the wall of inner cylinder. Therefore, the enthalpy balance is expressed as:

$$\Phi_1 = C_{p,c,1} \cdot \dot{m} \cdot (T_1 - T_i) = C_{p,h,1} \cdot \dot{m} \cdot (T_4 - T_o) \quad (1)$$

$$\Phi_1 = k_1 A_1 \frac{\Delta T_{\max} - \Delta T_{\min}}{\ln \frac{\Delta T_{\max}}{\Delta T_{\min}}}$$

(2)

$\Phi_1$  represents the specific heat absorbed by the air,  $C_{p,c,1}$  and  $C_{p,h,1}$  the average specific heat capacity of the air between cold and hot ends,  $\dot{m}$  mass flow rate,  $T_o$  and  $T_i$  outlet and inlet temperature,  $k_1$  heat transfer coefficient,  $A_1$  the surface area of phase 1,  $\Delta T_{\max}$  the maximum temperature difference between  $(T_o - T_i)$  and  $(T_4 - T_1)$ , and  $\Delta T_{\min}$  the minimum temperature difference.

Then, in the process of  $T_1 \rightarrow T_2$ , the heated air transfers heat through the wall of inner cylinder. The wall is both heated up by metal foam radiation and reflection of the metal foam solar radiation. Thus, the following relations can be established.

$$C_{p2} \cdot \dot{m} \cdot (T_2 - T_1) = h_w A_2 \frac{(T_w - T_1) - (T_w - T_2)}{\ln \left( \frac{T_w - T_1}{T_w - T_2} \right)}$$

(3)

$$C_{p2} \cdot \dot{m} \cdot (T_2 - T_1) = \varepsilon_w F_{fw} \{ \varepsilon_f A_f \sigma [(T_f + 273)^4 - (T_2 + 273)^4] + \rho_f \tau_g \eta_c A_c G \} \quad (4)$$

where  $C_{p2}$  stands for the average specific heat capacity of the air in the second process,  $\varepsilon_w$ ,  $T_w$  and  $A_w$  the emissivity, temperature and area of inner cylinder wall in the front part of the foam,  $\rho_f$ ,  $\varepsilon_f$ ,  $T_f$  and  $A_f$  the emissivity, temperature and area of the Ni-foam,  $F_{fw}$  the radiation shape factor between the foam and the wall of inner cylinder, and  $\sigma$  the blackbody radiation intensity valued  $5.67 \times 10^{-8} \text{ W}/(\text{m}^2 \cdot \text{C})$ .

In the succeeding process of  $T_2 \rightarrow T_3$ , the air flows through the outflow channel and flushes the inner surface of the quartz glass towards the window center, exchanging heat with the glass surface. Aside from the internal convective heat transfer on the inner wall of the glass, the natural convection on the outer wall, the radiation from incident sunlight, the reflected radiation from the foam, and the radiation from the inner cylinder surface are also dealt with in the proposed model.

$$C_{p3} \cdot \dot{m} \cdot (T_3 - T_2) = A_g h_{gi} \frac{(T_g - T_2) - (T_g - T_3)}{\ln\left(\frac{T_g - T_2}{T_g - T_3}\right)} \quad (5)$$

$$\begin{aligned} & \alpha_g I_b + \alpha'_g F_{fg} [\rho_f \tau_g I_b + \varepsilon_f A_f \sigma (T_f^4 - T_g^4)] + \alpha'_g F_{wg} \varepsilon_w A_w \sigma (T_w^4 - T_g^4) \\ & = \varepsilon'_g A_g \sigma (T_g^4 - T_a^4) + A_g h_{go} (T_g - T_a) + A_g h_{gi} \frac{(T_g - T_2) - (T_g - T_3)}{\ln\left(\frac{T_g - T_2}{T_g - T_3}\right)} \end{aligned}$$

(6)

where  $C_{p3}$  signifies the average specific heat capacity of the air in the third process,  $\alpha_g$ ,  $\tau_g$ ,  $T_g$ ,  $A_g$  the absorbance, transmissivity, temperature and area of the quartz glass at the wavelength of visible light,  $\alpha'_g$ ,  $\varepsilon'_g$  the absorbance and emissivity of the quartz glass under the long wave,  $F_{fg}$  the radiation shape factor between the foam and glass,  $F_{wg}$  the radiation shape factor between the surface of inner cylinder and glass,  $T_a$  the ambient temperature, and  $h_{go}$ ,  $h_{gi}$  the convective heat transfer coefficients of the outer and inner surface of the quartz

glass.

In the fourth process of  $T_3 \rightarrow T_4$ , the air flows into the metal foam and transfers the heat energy after flushing the inner surface of the glass,

$$C_{p4} \cdot \dot{m} \cdot (T_4 - T_3) = A_{sf} h_{sf} (T_f - T_{34}) \quad (7)$$

in which  $C_{p4}$  means the average specific heat capacity of the air in this process,  $A_{sf}$  and  $h_{sf}$  the surface area and convective heat transfer coefficient of the metal foam,  $T_{34}$  the average value of temperature between  $T_3$  and  $T_4$ . The last process of  $T_4 \rightarrow T_o$  is identical with the first one  $T_i \rightarrow T_1$ . The specific surface area of the metal foam  $A_{sf}$  is determined by the formula used in literature [14],

$$A_{sf} = \frac{3\pi d_f}{(0.59d_p)^2} [1 - \exp(-((1-\varphi)/0.04))] \quad (8)$$

where  $d_f$  denotes the thickness of the metal foam, which can be measured directly and calculated by the following formula,

$$\frac{d_f}{d_p} = 1.18 \sqrt{\frac{1-\varphi}{3\pi} \frac{1}{1 - \exp(-((1-\varphi)/0.04))}} \quad (9)$$

Radiant loss, convective loss and heat dissipative loss are the major heat loss forms of the entire receiver. Radiant loss concerns the loss of radiation from the quartz glass window and the chamber. Most of the convective loss is generated by the natural convection on the outer surface of the quartz glass window, while heat dissipative loss by the conduction through the insulations. Therefore, heat loss can be expressed as:

$$Q_{loss} = Q_{glass,emission} + Q_{glass,reflec\ tan\ ce} + Q_{foam,emission} + Q_{foam,reflec\ tan\ ce} + Q_{wall,emission} + Q_{convection} + Q_{conduction} \quad (10)$$

Since the thermal conductivity of the quartz glass is 1.46 w/(m•K), the thermal loss is small enough to be ignored. Other forms of heat loss can be calculated as follows,

$$Q_{glass,emission} = \varepsilon'_g A_g \sigma (T_g^4 - T_a^4) \quad (11)$$

$$Q_{glass,reflec\ tan\ ce} = \rho_g I_b \quad (12)$$

$$Q_{foam,emission} = \tau'_g F_{fg} \varepsilon_f A_f \sigma (T_f^4 - T_a^4) \quad (13)$$

$$Q_{foam,reflec\ tan\ ce} = \tau'_g F_{fg} \rho_f I_b \quad (14)$$

$$Q_{wall,emission} = \tau'_g F_{wg} \varepsilon_w A_w \sigma (T_w^4 - T_a^4) \quad (15)$$

$$Q_{convection} = A_g h_{go} (T_g - T_a) \quad (16)$$

Finally, the efficiency of the receiver is expressed as,

$$\eta_{receiver} = \frac{I_b - Q_{loss}}{I_b} \quad (17)$$

To calculate the efficiency of the receiver, parameters in the formulas should be determined, of which the most critical ones are  $T_g$ ,  $T_f$ , and  $T_w$ .

### 2.3. Heat transfer calculation

To examine the heat transfer process and calculate the efficiency of the receiver, the essential parameters in the above formulas should be obtained.

The radiant performance parameters of the quartz glass at visible and long wavelengths are obtained [30]. Due to the large porosity of mental foam, the effective emissivity is taken as 0.95. Being made of stainless steel, the surface of inner cylinder has emissivity of about 0.8 in the case of heavy oxidation. Relevant radiant performance parameters are summarized in Table 1.

Table 1 Radiant performance parameters.

|              |                               | emissivity | reflectivity | transmissivity |
|--------------|-------------------------------|------------|--------------|----------------|
| Quartz glass | Visible wave                  | 0.013      | 0.136        | 0.851          |
|              | Long wave                     | 0.326      | 0.125        | 0.549          |
|              | Mental foam                   | 0.95       | 0.05         | /              |
|              | The surface of inner cylinder | 0.8        | 0.2          | 0              |

Geometrical parameters, including the surface area of each component and the radiation shape factors, are also required. The area values are easy to be determined. As calculation of shape factors is complex, the geometrical structure between the metal foam surface and the flat window are simplified into two coaxial parallel discs; therefore, the radiation shape factors of the structure,  $F'_{fg}$ , can be expressed as,

$$R_1 = \frac{r_1}{L}, R_2 = \frac{r_2}{L}, S = 1 + \frac{1 + R_2^2}{R_1^2}, F_{1,2} = \frac{1}{2} \{ S - [S^2 - 4(R_2/r_1)^2]^{1/2} \} \quad (18)$$

in which  $r_1$  and  $r_2$  represent the radius of the first and second disc, and  $L$  the distance

between the discs. Similarly, the shape factors  $F_{fw}$  and  $F_{wg}$  can be determined. The calculated geometric parameters are summarized in Table 2.

Table 2 Results of geometric parameters.

| Parameter | $A_f$                | $A_g$                | $A_w$                | $F_{fg}$ | $F_{fw}$ | $F_{wg}$ |
|-----------|----------------------|----------------------|----------------------|----------|----------|----------|
| Value     | 0.1041m <sup>2</sup> | 0.0491m <sup>2</sup> | 0.1788m <sup>2</sup> | 0.3171   | 0.4340   | 0.1340   |

The first and second processes are assumed as forced convection in pipe. The outer surface of the glass for the third process is assumed as large-space natural convection, while the inner surface as forced convection on a flat plate. Besides, the fourth process is accepted as convective heat transfer in the metal foam. Therefore, the Nusselt number of the convective heat transfer in the first process, that is,  $Nu_1$ , could be determined with the Gnielinski Formula [31] expressed below,

$$Nu_1 = \frac{(f/8)(Re-1000)Pr_f}{1+12.7\sqrt{f/8}(Pr_f^{2/3}-1)} \left[1 + \left(\frac{d}{l}\right)^{2/3}\right] c_t \quad (19)$$

$$c_t = \left(\frac{T_f + 273}{T_w + 273}\right)^{0.45}, \frac{T_f + 273}{T_w + 273} = 0.5 \sim 1.5 \quad (20)$$

$$f = (1.82 \lg Re - 1.64)^{-2} \quad (21)$$

where  $l$  is the tube length and  $f$  the Darcy resistance coefficient. Similarly, the convective heat transfer coefficient between the air and the surface of inner cylinder in the second process, i.e.,  $Nu_2$ , can be calculated with Gnielinski Formula as well.

In the third phase, the Nusselt number of the natural convection on the outer surface can be computed as,

$$Nu_{3,m} = C(Gr \cdot Pr)_m^n \quad (22)$$

in which the values of  $C$ ,  $m$  and  $n$  depend on the Grashof number cited in reference [31]. The Nusselt number of the forced convection on the inner surface of the quartz glass ( $Nu_{3,l}$ ) is calculated with the heat transfer correlation of the thin layer flow of isothermal plate as,

$$Nu_{3,l} = 0.664 Re_l^{1/2} Pr^{1/3} \quad (23)$$

The convective heat transfer coefficient between the air and the metal foam in the fourth phase is determined by the Rukavuscass formula [32] listed below,

$$Nu_4 = \begin{cases} 0.74 Re^{0.4} Pr^{0.37}, & 1 \leq Re \leq 4 \\ 0.52 Re^{0.5} Pr^{0.37}, & 4 \leq Re \leq 10^3 \\ 0.26 Re^{0.6} Pr^{0.37}, & 10^3 \leq Re \leq 2 \times 10^5 \end{cases} \quad (24)$$

Solutions of  $T_g$ ,  $T_f$  and  $T_w$  depend on individual phases' air temperature. In phase 1,  $T_1$  and  $T_4$  can be calculated through calibration calculation steps of the receiver since  $T_i$ ,  $T_o$ ,  $k_1$  and  $A_1$  are known. Therefore, there are only five unknown temperature values:  $T_2$ ,  $T_3$ ,  $T_g$ ,  $T_f$ ,  $T_w$ , which can be simultaneously solved through Eqs.3-7 with iterative method. As all the unknown parameters in Eqs. 11-16 have been determined, the heat loss and efficiency of the solar receiver can be solved through Eqs. 10 and 17.

### 3. Results and discussions

#### 3.1. Model validation

The energy source of heat exchanger is mainly solar radiation, and the energy entering the solar receiver can be calculated when the technical parameters of the concentrator are known,

$$I_b = \eta_c A_c G \quad (25)$$

where  $I_b$  represents the energy entering the solar receiver,  $\eta_c$  and  $A_c$  the specular reflection efficiency and shadow area of the concentrator, and  $G$  the instantaneous solar radiation density.

The net energy absorbed by the receiver can be calculated by the temperature difference between the inlet and outlet of air flow,

$$Q_r = C_{av} \cdot \dot{m} \cdot (T_o - T_i) \quad (26)$$

where  $Q_r$  is the energy absorbed by the receiver, and  $C_{av}$  the average heat capacity of air inlet and outlet.

Therefore, the thermal efficiency of the solar receiver in the experiment can be obtained by calculating the ratio between the heat absorbed by the receiver and the heat entering the receiver:

$$\eta_{receiver} = \frac{Q_r}{I_b} = \frac{\dot{m} C_{av} (T_o - T_i)}{\eta_c A_c G} \quad (27)$$

Eqs. 27 is for calculating the experimental error of the receiver's heat efficiency, which reaches  $\mp 5.632\%$  according to the measuring instrument accuracy and error calculation formula of indirect measurement.

The existing solar receiver is located at Jianggan district, Hangzhou, Zhejiang province, China, with longitude of  $120.222^\circ$  and latitude of  $30.364^\circ$ . As presented in Fig. 3, the experimental

system of the solar receiver is composed of five subsystems: gas source, dish-shaped solar concentration part, solar receiver, pipeline system and data acquisition system. The air compressed by air pump flows into the receiver through pipe, and then the heated pressurized air is exhausted into the atmosphere. Data collection points are arranged in the pipe as well as the receiver, whose working pressure is five times higher than the atmosphere pressure. To limit the flow temperature variation between inlet and outlet (less than  $600^{\circ}\text{C}$ ), the minimum air flow rate is set around  $0.04\text{ kg/s}$ , the projected area of the solar concentrator around  $44\text{ m}^2$  and the optical efficiency  $86.45\%$ . Data acquisition system is designed for collecting and storing data of temperature, pressure, volume flow and direct solar radiant intensity transmitted through each measurement point in the solar receiver. Temperature measurement points are set on the outer wall, front & rear cover and the wall near the outlet (for correcting the outlet temperature error caused by thermal radiation). A pressure measurement point is also arranged near the flow measurement point. A vortex flowmeter is adopted to measure the volumetric flow of air, whose mass flow rate is obtained by virtue of the temperature and pressure data near the flowmeter. The experiment was conducted on November 5 and 6, 2015. The amount of radiation was estimated based on the solar radiation model mentioned in reference [33]. The direct solar radiation during daytime fluctuated considerably due to the heavy cloud, thus only the data collected on November 6 were selected. Values of air mass flux, efficiency and temperature of the outlet versus local time are shown in Fig. 4.



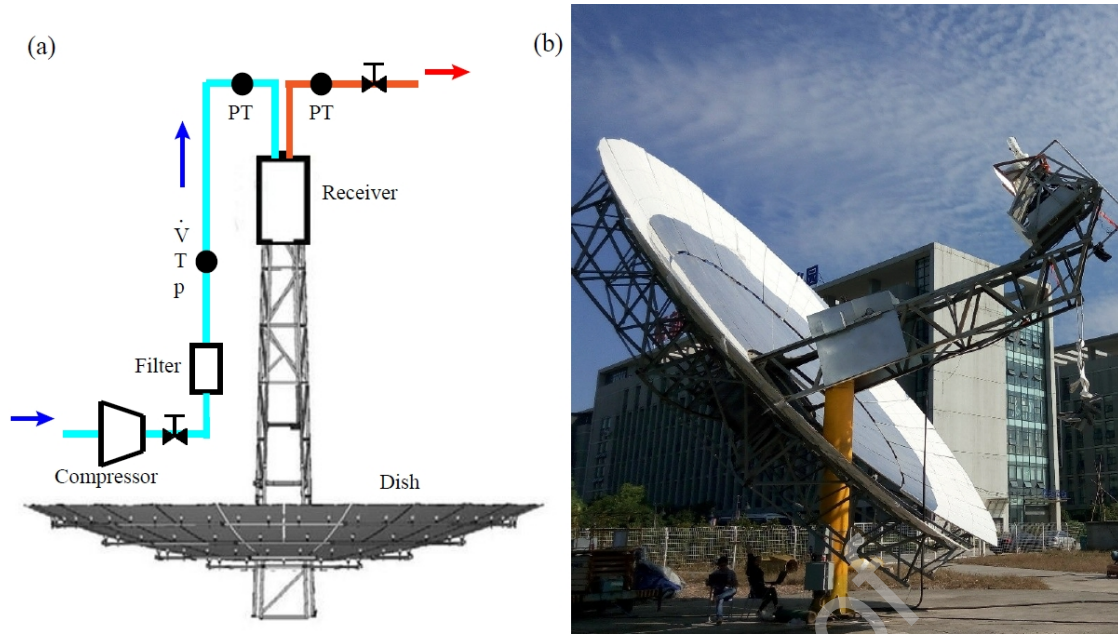


Figure 3: (a) Schematic diagram of the experimental system. (b) Photo of the experimental system

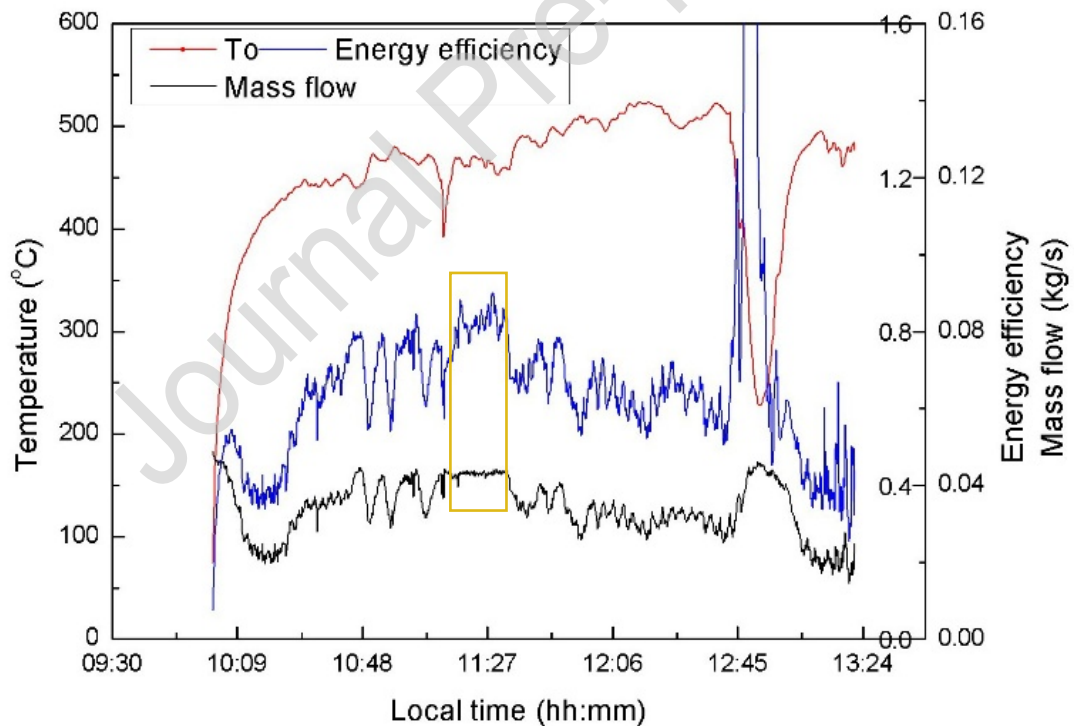


Figure 4: Variation of air mass flux, efficiency and temperature of the outlet.

Due to a sudden change of cloud cover and solar radiation intensity, the response lag of the measuring system may lead to an error: the sudden instantaneous efficiency is greater than 1 (for example, the efficiency measured at 12:47 to 12:52 is greater than 1). The efficiency measured at

the rest time fluctuates in the range of 30% to 85%. It can be observed that the data collected from 11:12 to 11:45 is relatively stable, thus is highlighted with yellow box in Fig. 4 for model validation. The air mass flux in this region reaches around 0.043 kg/s (2 Nm<sup>3</sup>/min), and corresponding energy efficiency 81.5%. The temperature values obtained in the experiment are used to calculate thermal parameters according to Eqs. 18-24. The results are shown in Table 3.

Table 3 Summary of thermal parameters

| parameter | $k_1$ | $h_w$ | $h_{gi}$ | $h_{go}$ | $h_{sf}$ | $A_{sf}$ |
|-----------|-------|-------|----------|----------|----------|----------|
| value     | 9.7   | 20.7  | 39       | 10       | 450      | 2023     |

As Eqs. 3-7 are nonlinear, matrix operation is replaced by iteration for easy calculation. The optimization algorithms used are quasi-Newton method and general global optimization method.

Table 4 displays the calculated temperature at each state.

Table 4 Temperature in each phase

| Temperature | $T_1$ | $T_2$ | $T_3$ | $T_4$ | $T_f$ | $T_w$ | $T_g$ |
|-------------|-------|-------|-------|-------|-------|-------|-------|
| Value       | 77.0  | 90.9  | 97.0  | 495.8 | 300.5 | 257.6 | 233.1 |

Heat losses of the solar receiver could be calculated with Eqs.10-15. Conductive losses were estimated according to the experimentally measured temperature of the outer surface of the receiver, where several temperature sensors were arranged. The estimated value of the heat dissipative loss provided by the experimental data was 2%. The total heat loss and energy efficiency were solved according to Eqs. 8-9. Specifically, the measured energy efficiency was 81.5%, while the predicted one was around 82.3%, suggesting good agreement between the two. Therefore, the proposed model is capable of accurately predicting the energy efficiency of the system.

### 3.2. Heat loss analysis

The experimental data and model prediction were identical on the condition of several

assumptions and approximations, thus more parameters should be referenced for further validation. Heat loss plays an important role in heat transfer experiments, which in turn increases the uncertainty of the experimental data, intensifying the necessity of heat loss analysis. The limitations of this simplified heat transfer model are summarized as follows. At first, obtained in the simplified geometry that was slightly different from the currently adopted geometry, all the equations used in the model are of empirical nature. Then, adoption of lumped temperature for each solid part leads to ignorance of the temperature variation inside each single component. In terms of radiation calculation, only the first-time reflection is considered. Besides, this model merely concerns the important features of the system that may substantially influence the heat transfer process. Moreover, it is assumed by this model that the air flows smoothly through the metal foam in phase 4. In particular, for calculation simplification, arithmetic mean value of temperature difference is utilized instead of instant temperature difference.

Despite the limitations, the heat loss results can still be used to analyze the performance of the current receiver. As described above, heat loss mainly consists of radiant loss, convective loss and conductive loss caused by heat dissipation. The share of each form of heat loss is illustrated in Fig. 5. It can be observed that the loss induced by the reflection on the quartz glass window constitutes the major part of heat losses, accounting for about 13.6% of the total energy loss; while the conduction loss caused by heat dissipation takes up around 2%, and the rest five losses (including radiant losses of the metal foam and the surface of the inner cylinder) around 1.4%.

The reflective property of the quartz glass material and shape of the quartz glass window are two dominant influencing factors on the reflective loss of the quartz glass window, of which the latter substantially influences the reflective efficiency. Generally, paraboloid-shaped or

cylindrical-typed quartz glass windows generate less reflective loss than the flat one. However, to lower cost and structural complexity, the flat one was chosen as the shape of quartz glass window in the experiment. High-quality quartz glass may reduce the reflectivity to about 7%. Hence, the reflective loss could be reduced by means of material improvement in future design.

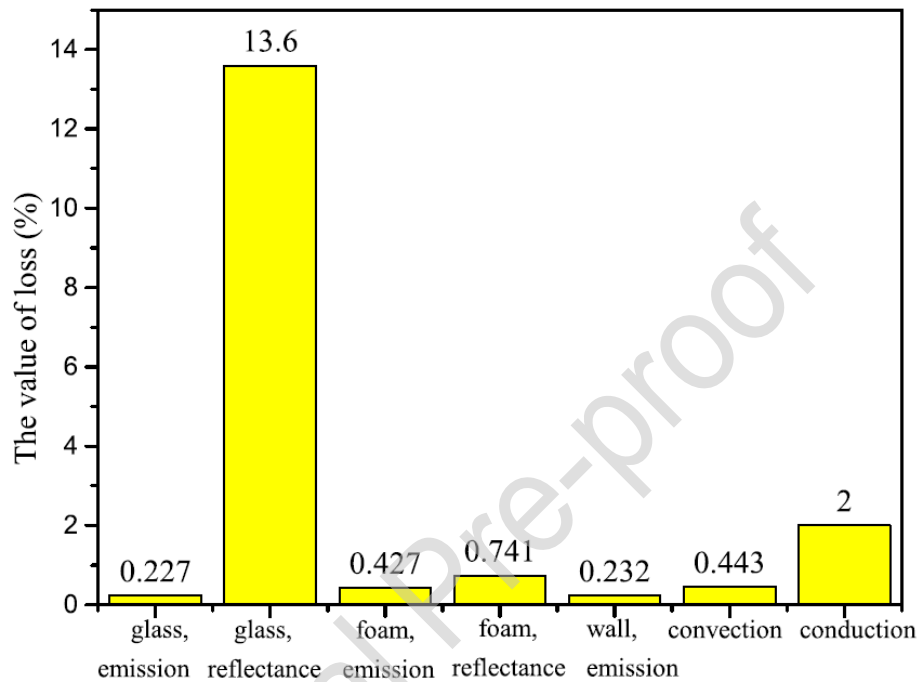


Figure 5: Shares of heat losses in the solar receiver.

Heat insulation and temperature distribution on the outer surface of the receiver are two dominant influencing factors on heat dissipation, of which the former is mainly influenced by thermal insulation materials, leaving little room for improvement. Temperature distribution depends on chamber structure and heat transfer structure, and improvement in the internal heat transfer structure may effectively curtail heat dissipation.

The radiation-induced heat loss is mainly influenced by chamber temperature. As long wave accounts for the major part of chamber radiation, and the quartz glass bears high reflectivity and absorptivity for long wave radiation, the radiation from the chamber is limited. In this case, radiant loss is controllable.

### 3.3. Model application

This simplified heat transfer model is highly conducive to solar receiver design as it is capable of estimating energy efficiency and heat loss. Its application may cover: the initial design before fabrication, fast performance prediction of different geometries for optimization, or the performance prediction of a given geometry under available conditions that experiments cannot reach. Heat loss analysis plays a key role in identifying major loss sources and presenting directions and suggestions for potential improvement and optimization.

The proposed model has broad prospects in application. The flow temperature at the rear of the solar receiver is crucial since it could be considered as the temperature of the hot end of a cycle, which in turn defines the cycle efficiency. Therefore, a higher outlet temperature is desired. One possible method is to enhance the inlet air temperature by adding a recuperator in front of the solar receiver inlet. In the present experiment, however, heat regenerator is absent as the experimental instruments and conditions are limited, the inlet air temperature is thus relatively low. Therefore, the performance of the solar receiver with high inlet temperature could be well predicted with this model.

The calculated values of air mass flux and incident solar radiation are identical with the experimental ones. The inlet temperature used in the model was from experimental measurement, whereas a rough estimation of outlet temperature was set as the initial value. The calculation was converged after 100 interactions. Simulations were performed under five varying working conditions, where inlet temperature ranged from 44 °C to 463 °C, and the results are listed in Figs. 6-8. The result of Case 1 is exactly the same with that of the experiment, whereas no experimental data is available for the other four cases with higher inlet air temperature.

Fig. 6 depicts variation of energy efficiency against the mean temperature ( $T_m$ ). A decreasing trend of energy efficiency is identified due to heat loss increment caused by high operation temperature. Specifically, the energy efficiency is around 82.3% when the mean experiment temperature reaches 250 °C, yet the number reduced to 73.9% when the mean temperature increased to 680.5 °C. The higher the mean temperature, the larger the absolute value of the slope. It is anticipated that further increase in the mean temperature accentuates decline of the energy efficiency. The radiant loss, in contrast, is elevating with mean temperature increment (see Fig. 7). Consisting of emissive loss of the quartz glass, metal foam, and inner cylinder surface, radiant loss takes up around 0.9% of the total energy loss in the experiment (Case 1), and rocks to 8.6% at the highest operation temperature. It can be concluded that the energy efficiency could be further improved in case of radiant loss reduction. Besides, the corresponding curve slope is increasing as the radiation magnitude augments according to the power law. Non-radiant heat loss mainly concerns the natural convection loss of the quartz glass. Fig. 8 uncovers that although non-radiant heat loss is increasing with  $T_m$ , the growth speed is dropping off. Accounting for merely less than 1.1% of the total energy loss in all the simulated cases, non-radiant heat loss could be neglected in a wide range of inlet air temperature.

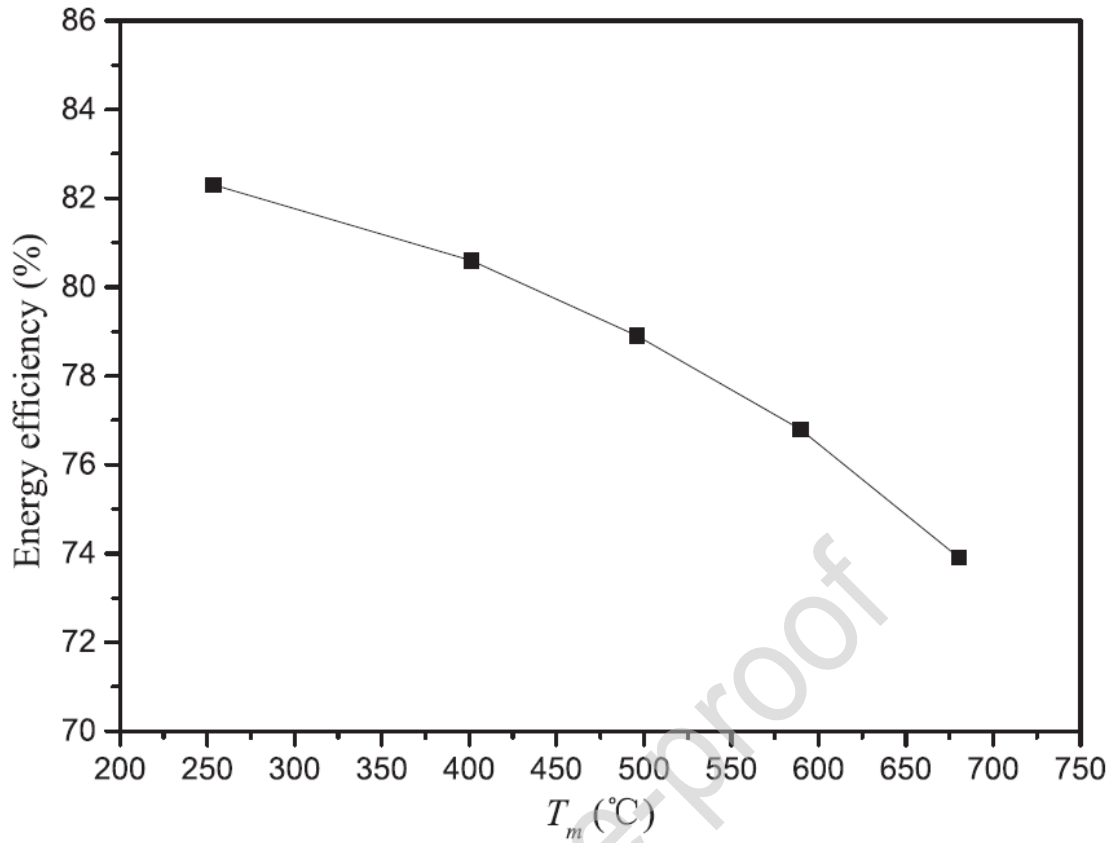


Figure 6: Variation of energy efficiency against mean temperature.

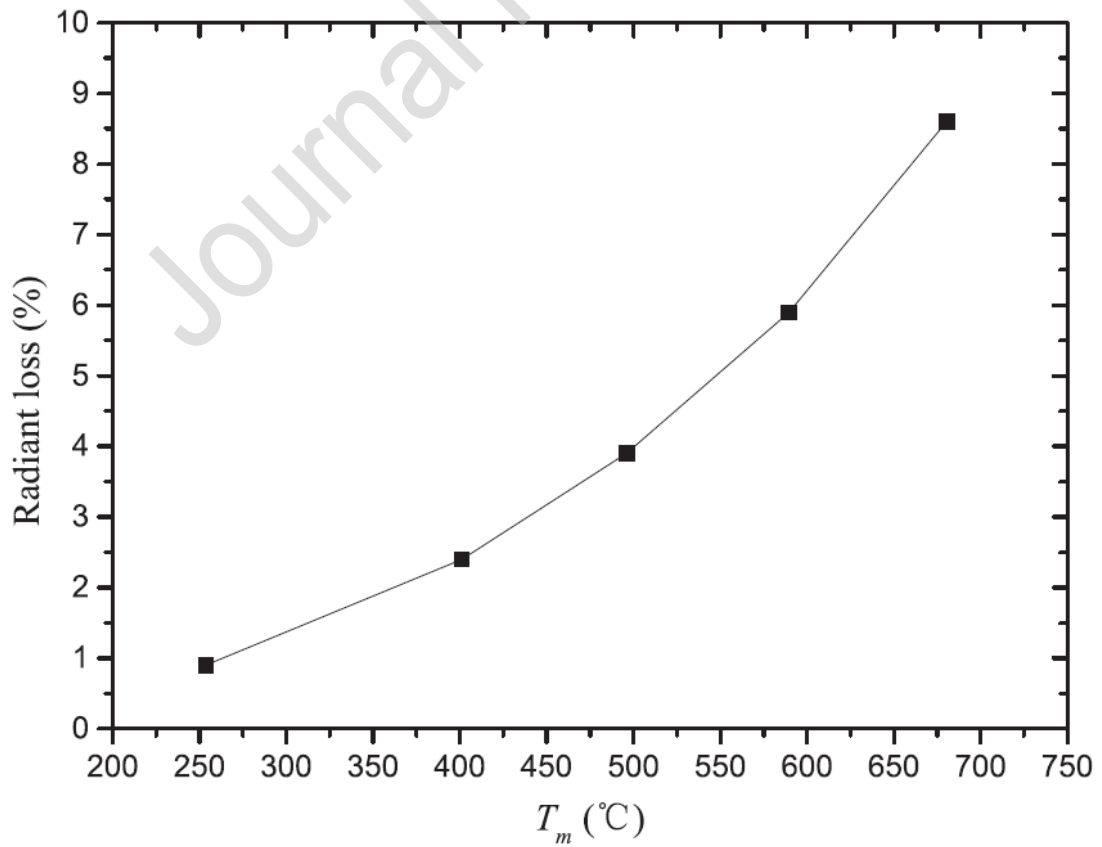
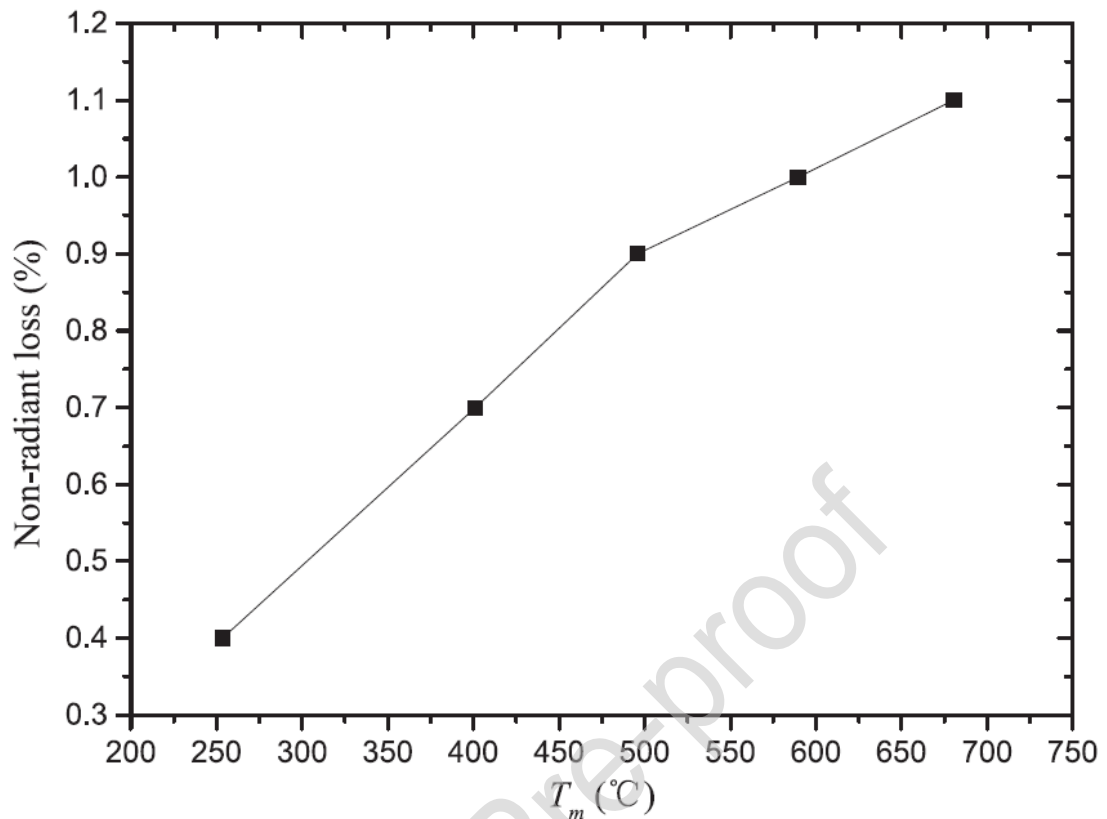


Figure 7: Variation of radiant loss against mean temperature.

Figure 8: Variation of non-radiant loss against  $T_m$ .

#### 4. Conclusions

This work presents a heat transfer model for solar receiver with metal foam by virtue of thermal computation and value comparison (with the available experimental data). Several heat transfer processes, including forced convection, natural convection, heat conduction and radiation, are analyzed. This model can be used for prediction of energy efficiency and percentage contribution of each form of heat loss. The results reveal good agreement between the predicted results and the experimental data. Further prediction of the performance of the solar receiver was carried out in the conditions out of the range of the experiments. It is concluded that inlet air temperature increment of the solar receiver may result in energy performance degradation and increase of radiant heat loss. Yet non-radiant heat loss accounts



for less than 1.1% of the total energy loss in all the simulated cases, indicating that the energy efficiency could be further improved in case of radiant loss reduction.

## Acknowledgement

The authors are grateful for the financial support from Royal Academy of Engineering (DVF1718\8\26), United Kingdom.

## References:

- [1] Zhu J, Kai W, Wu H, Wang D, Du J, Olabi AG. Experimental investigation on the energy and exergy performance of a coiled tube solar receiver. *Applied Energy*. 2015;156:519-27. <https://doi.org/10.1016/j.apenergy.2015.07.013>.
- [2] Roux WGL, Bello-Ochende T, Meyer JP. Operating conditions of an open and direct solar thermal Brayton cycle with optimized cavity receiver and recuperator. *Energy*. 2011;36:6027-36. <https://doi.org/10.1016/j.energy.2011.08.012>.
- [3] Kalogirou S. The potential of solar industrial process heat applications. *Applied Energy*. 2003;76:337-61. [https://doi.org/10.1016/s0306-2619\(02\)00176-9](https://doi.org/10.1016/s0306-2619(02)00176-9).
- [4] Tian Y, Zhao CY. A review of solar collectors and thermal energy storage in solar thermal applications. *Applied Energy*. 2013;104:538-53. <https://doi.org/10.1016/j.apenergy.2012.11.051>.
- [5] Yao Z, Wang Z, Lu Z, et al. Modeling and simulation of the pioneer 1 MW solar thermal central receiver system in China. *Renewable Energy*, 2009, 34(11):2437-2446. <https://doi.org/10.1016/j.renene.2009.02.022>.
- [6] Wang M, Siddiqui K. The impact of geometrical parameters on the thermal performance of a solar receiver of dish-type concentrated solar energy system. *Renewable Energy*. 2010;35:2501-13. <https://doi.org/10.1016/j.renene.2010.03.021>.
- [7] Grange B, Ferrie?Re A, Bellard D, Vrinat M, Couturier R, Pra F, et al. Thermal Performances of a High Temperature Air Solar Absorber Based on Compact Heat Exchange Technology. *Journal of Solar Energy Engineering*. 2011;133:031004. <https://doi.org/10.1115/1.4004356>.
- [8] Bader R, Pedretti A, Steinfeld A. Experimental and Numerical Heat Transfer Analysis of an Air-Based Cavity-Receiver for Solar Trough Concentrators. *Journal of Solar Energy Engineering*. 2012;134:519-28. <https://doi.org/10.1115/1.4005447>.
- [9] Bader R, Barbato M, Pedretti A, Steinfeld A. An Air-Based Cavity-Receiver for Solar Trough Concentrators. *Journal of Solar Energy Engineering*. 2010;132:1-7. <https://doi.org/10.1115/1.4001675>.
- [10] Wang K, Wu H, Wang D, Wang Y, Tong Z, Lin F, et al. Experimental study on a coiled tube solar receiver under variable solar radiation condition. *Solar Energy*. 2015;122:1080-90. <https://doi.org/10.1016/j.solener.2015.10.004>.
- [11] Wang Y, Wang K, Tong Z, Lin F, Nie C, Engeda A. Design and Optimization of a Single Stage Centrifugal Compressor for a Solar Dish-Brayton System. *Journal of Thermal Science*. 2013;22:404-12. <https://doi.org/10.1007/s11630-013-0642-x>.
- [12] Karsli S. Performance analysis of new-design solar air collectors for drying applications.

- Renewable Energy, 2007, 32(10):1645-1660. <https://doi.org/10.1016/j.renene.2006.08.005>.
- [13] Zhao CY. Review on thermal transport in high porosity cellular metal foams with open cells. *International Journal of Heat & Mass Transfer*. 2012;55:3618-32. <https://doi.org/10.1016/j.ijheatmasstransfer.2012.03.017>.
- [14] Calmidi VV, Mahajan RL. Forced Convection in High Porosity Metal Foams. *Journal of Heat Transfer*. 2000;122:557-65. <https://doi.org/10.1115/1.1287793>.
- [15] Mendes, M.A.A, Ray S, Trimis D. An improved model for the effective thermal conductivity of open-cell porous foams. *International Journal of Heat & Mass Transfer*, 2014, 75(75):224-230. <https://doi.org/10.1016/j.ijheatmasstransfer.2014.02.076>.
- [16] Kumar P, Topin F. Simultaneous determination of intrinsic solid phase conductivity and effective thermal conductivity of Kelvin like foams. *Applied Thermal Engineering*, 2014, 71(1):536-547. <https://doi.org/10.1016/j.applthermaleng.2014.06.058>.
- [17] Buck R, Bra?Uning T, Denk T, Pfander M, Schwarzbozl P, Tellez F. Solar-hybrid Gas turbine-based power tower systems (REFOS). *Journal of Solar Energy Engineering*. 2002;124:2-9. <https://doi.org/10.1115/1.1445444>.
- [18] Albanakis C, Missirlis D, Michailidis N, Yakinthos K, Goulas A, Omar H, et al. Experimental analysis of the pressure drop and heat transfer through metal foams used as volumetric receivers under concentrated solar radiation. *Experimental Thermal & Fluid Science*. 2009;33:246-52. <https://doi.org/10.1016/j.expthermflusci.2008.08.007>.
- [19] Michailidis N, Stergioudi F, Omar H, Missirlis D, Vlahostergios Z, Tsipas S, et al. Flow, thermal and structural application of Ni-foam as volumetric solar receiver. *Solar Energy Materials & Solar Cells*. 2013;109:185-91. <https://doi.org/10.1016/j.solmat.2012.10.021>.
- [20] He Y L, Xiao J, Cheng Z D, et al. A MCRT and FVM coupled simulation method for energy conversion process in parabolic trough solar collector. *Renewable Energy*, 2011, 36(3):976-985. <https://doi.org/10.1016/j.renene.2010.07.017>.
- [21] Wu Z, Wang Z. Fully coupled transient modeling of ceramic foam volumetric solar air receiver. *Solar Energy*. 2013;89:122-33. <https://doi.org/10.1016/j.solener.2012.12.016>.
- [22] Chen X, Xia XL, Meng XL, Dong XH. Thermal performance analysis on a volumetric solar receiver with double-layer ceramic foam. *Energy Conversion & Management*. 2015;97:282-9. <https://doi.org/10.1016/j.enconman.2015.03.066>.
- [23] Hischer I. Experimental and Numerical Analyses of a Pressurized Air Receiver for Solar-Driven Gas Turbines. *Journal of Solar Energy Engineering*. 2012;134:021003. <https://doi.org/10.1115/1.4005446>.
- [24] Hess D, Lipiski W, Modest M, Steinfeld A. Heat Transfer Analysis of a Novel Pressurized Air Receiver for Concentrated Solar Power via Combined Cycles. *Journal of Thermal Science & Engineering Applications*. 2009;1:105-12. <https://doi.org/10.1115/1.4001259>.
- [25] Hischer I, Poživil P, Steinfeld A. A Modular Ceramic Cavity-Receiver for High-Temperature High-Concentration Solar Applications. *Journal of Solar Energy Engineering*. 2012;134:011004. <https://doi.org/10.1115/1.4005107>.
- [26] Poživil, Aga V, Zagorskiy A, Steinfeld A. A Pressurized Air Receiver for Solar-driven Gas Turbines. *Energy Procedia*. 2014;49:498-503. <https://doi.org/10.1016/j.egypro.2014.03.053>.

- [27] Lim S, Kang Y, Lee H, Shin S. Design optimization of a tubular solar receiver with a porous medium. *Applied Thermal Engineering*. 2014;62:566-72. <https://doi.org/10.1016/j.applthermaleng.2013.10.025>.
- [28] Weigel P. Development and piloting of a pressurized volumetric solar heat receiver designed to run with a Brayton cycle gas turbine: Leibniz University; 2013.
- [29] Mortazavi B , Yang H , Mohebbi F , et al. Graphene or h-BN paraffin composite structures for the thermal management of Li-ion batteries: A multiscale investigation[J]. *Applied Energy*, 2017, 202:323-334. <https://doi.org/10.1016/j.apenergy.2017.05.175>.
- [30] Röger M, Rickers C, Uhlig R, Neumann F, Polenzky C. Infrared-Reflective Coating on Fused Silica for a Solar High-Temperature Receiver. *Journal of Solar Energy Engineering, Transactions of the ASME*, May 2009, 131(2):0210041-0210047. <https://doi.org/10.1115/1.3097270>.
- [31] Yang S, Tao W. *Heat Transfer*, fourth ed. Beijing: Higher Education Press; 2012.
- [32] Zhao CY, Kim T, Lu TJ, Hodson HP. Thermal Transport in High Porosity Cellular Metal Foams. *Journal of Thermophysics & Heat Transfer*. 2004;18:309-17. <https://doi.org/10.2514/1.11780>.
- [33] Wong LT, Chow WK. Solar radiation model. *Applied Energy*. 2001;69:191-224. [https://doi.org/10.1016/s0306-2619\(01\)00012-5](https://doi.org/10.1016/s0306-2619(01)00012-5).

#### Research Highlight

1. A novel model is developed to investigate the heat transfer process in a solar receiver with porous medium;
2. The forced and natural convection, heat conduction and radiation is considered in the proposed model;
3. The proposed model can predict the energy efficiency efficiently and accurately;
4. The model can be further used to design and optimize the solar receiver.

Journal Pre-proof